

## ROTATING STARBURST CORES IN MASSIVE GALAXIES AT $Z = 2.5$

KEN-ICHI TADAKI<sup>1</sup>, TADAYUKI KODAMA<sup>2,3</sup>, ERICA J. NELSON<sup>1</sup>, SIRIO BELLI<sup>1</sup>, NATASCHA M. FÖRSTER SCHREIBER<sup>1</sup>,  
REINHARD GENZEL<sup>1,4,5</sup>, MASAO HAYASHI<sup>2</sup>, RODRIGO HERRERA-CAMUS<sup>1</sup>, YUSEI KOYAMA<sup>6</sup>, PHILIPP LANG<sup>7</sup>, DIETER LUTZ<sup>1</sup>,  
RHYTHM SHIMAKAWA<sup>3</sup>, LINDA J. TACCONI<sup>1</sup>, HANNAH ÜBLER<sup>1</sup>, EMILY WISNIOSKI<sup>1</sup>, STIJN WUYTS<sup>8</sup>, BUNYO HATSUKADE<sup>9</sup>,  
MAGDALENA LIPPA<sup>1</sup>, KOUICHIRO NAKANISHI<sup>2,3</sup>, SOH IKARASHI<sup>10</sup>, KOTARO KOHNO<sup>9,11</sup>, TOMOKO L. SUZUKI<sup>3</sup>, YOICHI  
TAMURA<sup>9</sup>, AND ICHI TANAKA<sup>6</sup>

<sup>1</sup> Max-Planck-Institut für extraterrestrische Physik, Giessenbachstrasse, D-85748 Garching, Germany; tadaki@mpe.mpg.de

<sup>2</sup> National Astronomical Observatory of Japan, 2-21-1 Osawa, Mitaka, Tokyo 181-8588, Japan

<sup>3</sup> Department of Astronomical Science, SOKENDAI (The Graduate University for Advanced Studies), Mitaka, Tokyo 181-8588, Japan

<sup>4</sup> Department of Physics, Le Conte Hall, University of California, Berkeley, CA 94720, USA

<sup>5</sup> Department of Astronomy, Hearst Field Annex, University of California, Berkeley, CA 94720, USA

<sup>6</sup> Subaru Telescope, National Astronomical Observatory of Japan, 650 North A'ohoku Place, Hilo, HI 96720, USA

<sup>7</sup> Max-Planck-Institut für Astronomie, Königstuhl 17, D-69117 Heidelberg, Germany

<sup>8</sup> Department of Physics, University of Bath, Claverton Down, Bath, BA2 7AY, UK

<sup>9</sup> Institute of Astronomy, The University of Tokyo, 2-21-1 Osawa, Mitaka, Tokyo 181-0015, Japan

<sup>10</sup> Kapteyn Astronomical Institute, University of Groningen, P.O. Box 800, 9700AV Groningen, The Netherlands and

<sup>11</sup> Research Center for the Early Universe, The University of Tokyo, 7-3-1 Hongo, Bunkyo, Tokyo 113-0033, Japan

*Draft version November 26, 2018*

### ABSTRACT

We present spatially resolved ALMA observations of the CO  $J = 3 - 2$  emission line in two massive galaxies at  $z = 2.5$  on the star-forming main sequence. Both galaxies have compact dusty star-forming cores with effective radii of  $R_e = 1.3 \pm 0.1$  kpc and  $R_e = 1.2 \pm 0.1$  kpc in the 870  $\mu\text{m}$  continuum emission. The spatial extent of star-forming molecular gas is also compact with  $R_e = 1.9 \pm 0.4$  kpc and  $R_e = 2.3 \pm 0.4$  kpc, but more extended than the dust emission. Interpreting the observed position-velocity diagrams with dynamical models, we find the starburst cores to be rotation-dominated with the ratio of the maximum rotation velocity to the local velocity dispersion of  $v_{\text{max}}/\sigma_0 = 7.0^{+2.5}_{-2.8}$  ( $v_{\text{max}} = 386^{+36}_{-32}$  km s<sup>-1</sup>) and  $v_{\text{max}}/\sigma_0 = 4.1^{+1.7}_{-1.5}$  ( $v_{\text{max}} = 391^{+54}_{-41}$  km s<sup>-1</sup>). The comparisons among dynamical, stellar, gas, and dust mass suggest that the starburst CO-to-H<sub>2</sub> conversion factor of  $\alpha_{\text{CO}} = 0.8 M_{\odot} (\text{K km s}^{-1} \text{pc}^{-2})^{-1}$  is appropriate in the spatially resolved cores. The dense cores are likely to be formed in extreme environments similar to the central regions of local ultraluminous infrared galaxies. Given their short gas depletion timescale of  $46 \pm 11$  Myr and  $79 \pm 46$  Myr, they are likely to be the immediate progenitors of bulge-dominated quiescent galaxies. Our work also demonstrates that a combination of medium-resolution CO and high-resolution dust continuum observations is a powerful tool for characterizing the dynamical state of molecular gas in distant galaxies.

*Subject headings:* galaxies: evolution — galaxies: high-redshift — galaxies: ISM

### 1. INTRODUCTION

Massive quiescent galaxies often have dense cores with stellar mass surface densities reaching  $10^{10} M_{\odot} \text{kpc}^{-2}$  (Fang et al. 2013; van Dokkum et al. 2014). In contrast, the morphology of star-forming galaxies is typically dominated by extended, exponential disks rather than central bulges (e.g., Wuyts et al. 2011a). Massive star-forming galaxies are expected to form a dense core and transform their morphology from disk-dominated to bulge-dominated before quenching their star formation. Understanding the formation history of the bulge component is a critical step toward revealing the origin of the Hubble sequence. At the peak epoch of galaxy formation ( $z \sim 2$ ), the most massive,  $\log(M_*/M_{\odot}) > 11$ , star-forming galaxies still have extended disks, but are rapidly building up their central cores through dusty, compact starbursts (Tadaki et al. 2017; Barro et al. 2016). Bulge formation in a short period of less than 1 Gyr at  $z \sim 2$  is also corroborated by observations of old stellar populations and enhanced  $[\alpha/\text{Fe}]$  ratios in massive quiescent galaxies at  $z \sim 1$  (e.g., Belli et al. 2015; Onodera et al. 2015). All these findings suggest that central cores of massive galaxies have a different formation history than

outer disks and less massive galaxies. The next step is to characterize the kinematics of these dense cores in the process of formation, which will shed light on their formation mechanisms and subsequent evolution.

At high-redshift, the kinematics of dusty star-forming cores in massive galaxies are difficult to study. While H $\alpha$  studies with near-infrared spectrographs have made significant progress in understanding the kinematics of core formation (e.g., Nelson et al. 2014; Barro et al. 2014; E. Wisnioski et al. 2017, in preparation), the H $\alpha$  line is not an ideal tool for investigating the kinematics of forming cores because of dust attenuation. Multi-wavelength high-resolution imaging and emission line maps from grism spectroscopy reveal that the central regions in massive high-redshift galaxies are often strongly attenuated by dust (Wuyts et al. 2012; Nelson et al. 2016). CO line observations provide a more robust means of obtaining kinematic information for dusty objects, as well as the molecular gas properties (e.g., Tacconi et al. 2008; Ivison et al. 2013).

In local ultraluminous infrared galaxies (ULIRGs), molecular gas is concentrated into rotating nuclear disks or rings (e.g., Downes & Solomon 1998). Moreover, the

physical condition of the gas is totally different from that in normal star-forming galaxies. In normal star-forming regions, CO emission mainly comes from an ensemble of self-gravitating molecular clouds. Although the CO line is typically optically thick in each virialized molecular cloud, it is possible to count the number of clouds and estimate the total molecular gas mass. We use the CO-to-H<sub>2</sub> conversion factor of  $\alpha_{\text{CO}} = M_{\text{gas}}/L'_{\text{CO}} = 4.36 M_{\odot} (\text{K km s}^{-1} \text{pc}^{-2})^{-1}$  including a correction for Helium since it is calibrated by virial mass measurements, optically thin dust emission and  $\gamma$ -ray observations in the Milky-Way disk (see review in Bolatto et al. 2013).

A CO-based gas mass with the Galactic conversion factor, however, often equals or exceeds a dynamical mass in local ULIRGs and SMGs, which could imply a smaller conversion factor (e.g., Downes & Solomon 1998; Tacconi et al. 2008). This variation of  $\alpha_{\text{CO}}$  could be caused by a high star formation rate (SFR) surface density in extreme environments. The intense UV radiation heats the nearby dust and the gas temperature increases through efficient energy exchange with hot dust (Narayanan et al. 2012). Then, the CO surface brightness increases more rapidly than the gas mass surface density.

In this letter, we report results from CO  $J = 3 - 2$  observations of two massive galaxies at  $z = 2.5$  using Atacama Large Millimeter/submillimeter Array (ALMA) to study the spatial distribution and the kinematics of molecular gas in the starburst cores. We assume a Chabrier initial mass function (IMF; Chabrier 2003) and adopt cosmological parameters of  $H_0 = 70 \text{ km s}^{-1} \text{ Mpc}^{-1}$ ,  $\Omega_{\text{M}} = 0.3$ , and  $\Omega_{\Lambda} = 0.7$ .

## 2. OBSERVATIONS

We select two galaxies at  $z = 2.53$  (U4-16795 and U4-16504) from Subaru narrow-band imaging in the SXDF field (Tadaki et al. 2013). They lie close to each other and their projected separation is  $9''.7$  (78 kpc in physical scale) within the primary beam of ALMA Band-3 receivers (a beam width at half power of  $\sim 1'$ ). Both galaxies have a compact dusty star-forming core, which is probed by  $870 \mu\text{m}$  dust continuum emission (Tadaki et al. 2017). We compute the stellar mass using the FAST spectral energy distribution fitting code (Kriek et al. 2009) and the 3D-HST multi-wavelength photometric catalog (Skelton et al. 2014) using the stellar population synthesis models of Bruzual & Charlot (2003), exponentially declining star formation histories, and dust attenuation law of Calzetti et al. (2000). The total stellar mass is  $\log(M_*/M_{\odot}) = 11.26 \pm 0.15$  for U4-16795 and  $\log(M_*/M_{\odot}) = 11.25 \pm 0.15$  for U4-16504. In deep HAWK-I/ $K_s$ -band maps (Fontana et al. 2014), 81% and 71% of the total fluxes come from the central  $1''.5$  aperture region for U4-16795 and U4-16504, respectively. We take into account these factors when comparing the stellar mass with other masses (Section 4.2).

U4-16795 is detected in a deep *Herschel*-PACS  $160 \mu\text{m}$  map from archival data (see Lutz et al. 2011 for the methodology) and U4-16504 is detected in a deep *Spitzer*-MIPS  $24 \mu\text{m}$  map (PI: J. Dunlop). Following the recipes of Wuyts et al. (2011b), we derive SFRs of  $\log(\text{SFR}/M_{\odot}\text{yr}^{-1}) = 2.62 \pm 0.1$  for U4-16795 and  $\log(\text{SFR}/M_{\odot}\text{yr}^{-1}) = 2.37 \pm 0.25$  for U4-16504 from

a combination of the rest-frame  $2800 \text{ \AA}$  and infrared luminosities. The targets are located on the massive end of the star-forming main sequence at  $z \sim 2$  (e.g., Speagle et al. 2014).

We observe the CO  $J = 3 - 2$  emission line ( $\nu_{\text{rest}} = 345.796 \text{ GHz}$ ) of the two massive galaxies with ALMA Band-3 receivers covering the frequency range of 95–99 and 107–111 GHz. The calibration is processed through the Common Astronomy Software Application package (CASA; McMullin et al. 2007). We use the `tclean` task with natural weighting to make a channel map with a velocity width of  $50 \text{ km s}^{-1}$  and dirty continuum maps excluding the frequency range of the CO line. The synthesized beams are  $0''.66 \times 0''.55$ . The rms levels are  $147 \mu\text{Jy beam}^{-1}$  in the channel map and  $8.1 \mu\text{Jy beam}^{-1}$  in the continuum map.

## 3. RESULTS AND ANALYSIS

We robustly detect CO  $J = 3 - 2$  emission in both galaxies as seen in the spatially-averaged spectra within a  $1''.5$  aperture (Figure 1). We measure total fluxes within a  $1''.5$  aperture in the velocity-integrated maps to derive the CO line luminosities (Table 1). Both galaxies show a spatial offset between the blue- and red-shifted CO components with a velocity width of  $150 \text{ km s}^{-1}$  (Figure 1). The two central positions determine the kinematic major axis of the molecular gas disks. We also derive line-of-sight velocities by fitting a Gaussian function to the CO line spectrum in each spatial pixel. The velocity field maps show a monotonic gradient along the kinematic major axis (Figure 1), suggesting rotation of the molecular gas. In this section, we construct the dynamical model of the dusty star-forming cores through the following three steps: (1) determining a minor-to-major axis ratio ( $q = b/a$ ) of the  $870 \mu\text{m}$  continuum emission, (2) measuring an effective radius ( $R_e$ ) of the CO line emission, and (3) exploring the best-fit dynamical model.

### 3.1. Spatial extent of dust

$0''.2$ -resolution  $870 \mu\text{m}$  continuum maps are available for both galaxies (Tadaki et al. 2017). In SMGs at high-redshift, the dust emission is well described by an elliptical exponential disk (Hodge et al. 2016). We derive effective radii,  $R_e$ , along the major axis of the  $870 \mu\text{m}$  continuum emission assuming an elliptical disk while Tadaki et al. (2017) have adopted circular disk models ( $q = 1$ ). We use the `UVMULTIFIT` tool to fit the visibility amplitudes to models in the  $u - v$  plane (Martí-Vidal et al. 2014). For U4-16795, the best-fit values and fitting errors are  $R_e = 1.3 \pm 0.1 \text{ kpc}$ ,  $q = 0.49 \pm 0.07$  and position angle of  $\text{PA}_{\text{mor}} = 35^\circ \pm 5^\circ$ . Note that the morphological major axis of the  $870 \mu\text{m}$  continuum emission is well aligned with the kinematics major axis of the CO line emission ( $|\text{PA}_{\text{mor}} - \text{PA}_{\text{kin}}| = 8^\circ$ ), supporting ordered rotation. We also perform the visibility fitting for U4-16504 with an elliptical disk, but could not obtain meaningful constraints on the axis ratio. Circular disk models give an effective radius of  $R_e = 1.2 \pm 0.1 \text{ kpc}$ .

### 3.2. Spatial extent of molecular gas

Next, we derive effective radii of the CO line emission using the axis ratio of the dust emission. We fix the minor-to-major axis ratio to  $q = 0.49$  and  $\text{PA}_{\text{mor}} = 35^\circ$

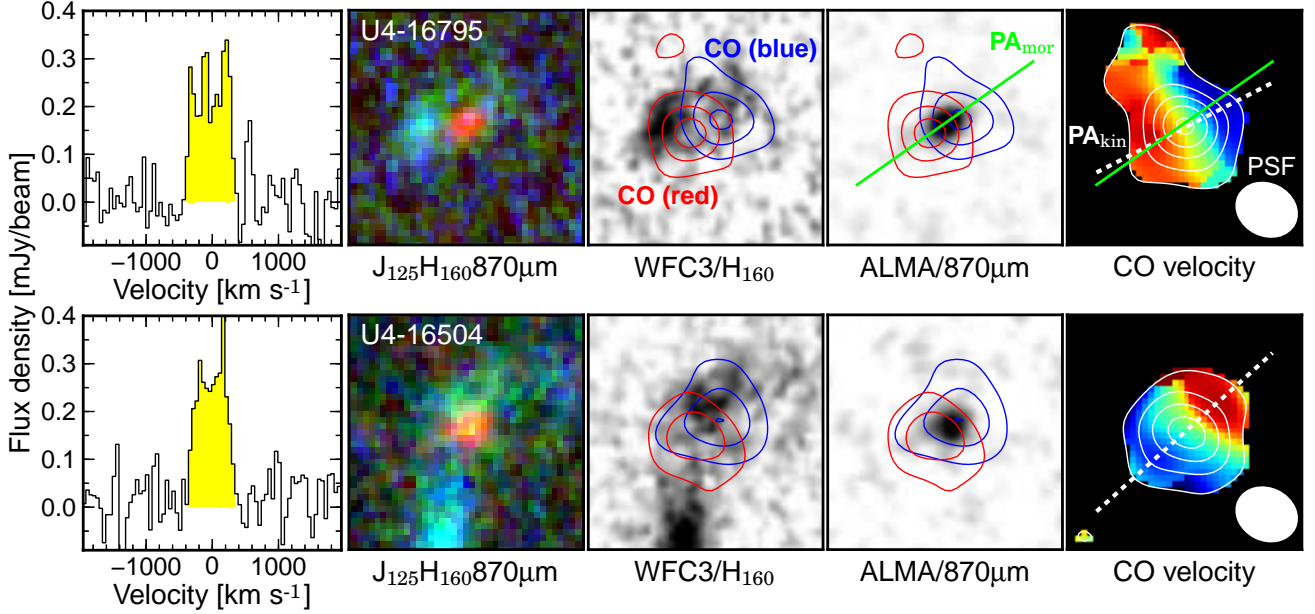


FIG. 1.— Spatially-averaged CO  $J = 3 - 2$  spectra and HST/F125W-, F160W-, and ALMA/870  $\mu\text{m}$ -band maps ( $2''.5 \times 2''.5$ ) for two massive star-forming galaxies at  $z = 2.5$ . Red, blue and white contours display blue- and red-shifted CO components with a velocity width of  $150 \text{ km s}^{-1}$  and the velocity-integrated CO fluxes every  $3\sigma$ , respectively. The right-most panels are maps of the CO velocity field. Green and white dashed lines indicate the morphological major axis of 870  $\mu\text{m}$  continuum emission and the kinematic major axis of CO, respectively.

TABLE 1  
GALAXY PROPERTIES FOR TWO MASSIVE STAR-FORMING GALAXIES AT  $z = 2.5$ .

ID	$z_{\text{CO}}$	$S_{\text{CO}} dv^a$ (Jy km s $^{-1}$ )	$\log L'_{\text{CO}(3-2)}$ (K km s $^{-1}$ pc $^{-2}$ )	$\log M_{\text{dyn}}$ ( $M_{\odot}$ )	$\log M_{*}^b$ ( $M_{\odot}$ )	$\log M_{\text{gas,CO}}^b$ ( $M_{\odot}$ ) [ $\alpha_{\text{CO}} = 4.36$ ]	$\log M_{\text{gas,CO}}^b$ ( $M_{\odot}$ ) [ $\alpha_{\text{CO}} = 0.8$ ]	$\log M_{\text{gas,3mm}}^c$ ( $M_{\odot}$ ) [ $\delta_{\text{gdr}} = 120$ ]
U4-16795	2.5236	$0.72 \pm 0.06$	$10.37 \pm 0.04$	$11.10^{+0.13}_{-0.12}$	$11.17 \pm 0.15$	$11.01 \pm 0.04$	$10.28 \pm 0.04$	$10.38 - 10.96$
U4-16504	2.5267	$0.72 \pm 0.05$	$10.37 \pm 0.03$	$11.19^{+0.17}_{-0.15}$	$11.10 \pm 0.15$	$11.01 \pm 0.03$	$10.27 \pm 0.03$	$10.41 - 10.98$

<sup>a</sup> Velocity-integrated CO fluxes within the  $1''.5$  aperture. The uncertainties are estimated from the standard deviation of 200 random aperture photometry measurements.

<sup>b</sup> Stellar mass and CO-based gas mass within the  $1''.5$  aperture.

<sup>c</sup> The  $5\sigma$  limit of 3 mm continuum-based gas mass within the  $1''.5$  aperture through the gas-to-dust ratio of 120. The range corresponds to the dust emissivity of  $\kappa_{850} = 0.4 - 1.5 \text{ g}^{-1} \text{ cm}^2$ .

for U4-16795, and to  $q = 1$  (circular disk) for U4-16504. Figure 2 shows the observed visibility amplitudes and the best-fit models. The effective radii are  $R_e = 1.9 \pm 0.4$  kpc for U4-16795 and  $R_e = 2.3 \pm 0.4$  kpc for U4-16504. The star-forming molecular gas is more compact than the rest-optical emission of massive star-forming galaxies at similar redshift ( $R_e = 4.4^{+2.4}_{-1.5}$  kpc; van der Wel et al. 2014a). On the other hand, the CO size is larger than the size of dust emission, suggesting that the molecular gas disks host more compact dusty star-forming cores.

### 3.3. Molecular gas kinematics

We find that both massive galaxies observed here display evidence for rotating disks of molecular gas in their CO velocity fields (Figure 1). The velocity gradient seen in the position-velocity (PV) diagram along the kinematic major axis is consistent with rotation (Figure 3). We investigate the kinematic properties of the gas disks by fitting dynamical models to the data. We use the DYSMAL code (Davies et al. 2011) to generate PV diagrams for an exponential disk, spatially convolved with

a  $0''.66 \times 0''.55$  Gaussian beam. We take into account the effect of pressure support, reducing the observed rotation velocity (e.g., Wuyts et al. 2016; Burkert et al. 2010). The effective radii of the gas disks are fixed to the values measured in Section 3.2. For U4-16795, we infer an inclination,  $i$ , from the axis ratio of the 870  $\mu\text{m}$  dust continuum emission as  $\sin^2 i = (1 - q^2)/(1 - \text{thickness}^2)$  for symmetric oblate disks with an intrinsic thickness of 0.25 (van der Wel et al. 2014b). The inclination is  $\log(1/\sin^2 i) = 1.11 \pm 0.04$  dex (corresponding to  $i = 64^\circ$ ). This uncertainty propagates to the dynamical mass estimate as  $M_{\text{dyn}} \propto 1/\sin^2 i$ . As the effective radius and the inclination are fixed, the remaining free parameters in the model are dynamical mass,  $M_{\text{dyn}}$ , and local velocity dispersion,  $\sigma_0$ . For U4-16504, we assume an average inclination of  $\sin i = 0.79$  ( $i = 52^\circ$ ) in the case of isotropically oriented disks (see Appendix of Law et al. 2009). As the deviation is derived as  $(\int (\sin i - 0.79)^2 \sin i di / \int \sin i di)^{1/2} = 0.22$  ( $i = 35^\circ - 90^\circ$ ), we adopt the uncertainty of  $\Delta \log(1/\sin^2 i) = \pm 0.09$  dex.

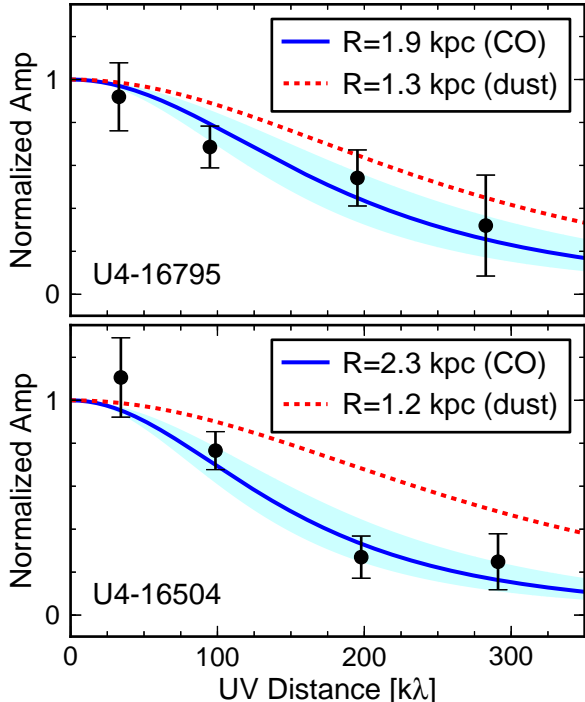


FIG. 2.— Visibility amplitudes of the velocity-integrated CO emission for U4-16795 (top) and U4-16504 (bottom). The blue solid line and the shaded region indicate the best-fitting model and the  $1\sigma$  error, respectively. The red dashed line presents the best-fitting model of the  $870\ \mu\text{m}$  dust emission. The x-axis gives the circularized uv distance.

In the PV diagrams, we use the pixels with a flux above  $3\sigma$  to calculate the chi-squared values between the data and the models. Figure 3 shows the best-fit models to minimize the chi-squared value along with the residual maps after subtracting the model from the data. The best fit models for the two galaxies have dynamical masses  $\log(M_{\text{dyn}}/M_{\odot}) = 11.10^{+0.07}_{-0.06}$  for U4-16795 and  $\log(M_{\text{dyn}}/M_{\odot}) = 11.19^{+0.12}_{-0.09}$  for U4-16504. These uncertainties are based on the reduced-chi squared values corresponding to a p-value above 5%. In the dynamical mass measurements, after taking into account the uncertainties of effective radius and inclination, our final uncertainties are  $+0.13$  dex ( $-0.12$  dex) for U4-16795 and  $+0.17$  dex ( $-0.15$  dex) for U4-16504.

We also derive values for the crucial kinematic properties, rotation velocity and local velocity dispersion, from the best fit models. We find  $v_{\text{max}} = 386^{+36}_{-32}$   $\text{km s}^{-1}$  and  $\sigma_0 = 55^{+19}_{-22}$  for U4-16795 and  $v_{\text{max}} = 391^{+54}_{-41}$   $\text{km s}^{-1}$  and  $\sigma_0 = 96^{+35}_{-31}$   $\text{km s}^{-1}$  for U4-16504. We note that they have a larger local velocity dispersion than the mean value ( $\sigma_0=50$   $\text{km s}^{-1}$ ) in a large sample of rotation-dominated galaxies at  $z \sim 2$  (Wisnioski et al. 2015). This means that both dusty star-forming cores are rotation-dominated with the ratio of the maximum rotation velocity to local velocity dispersion of  $v_{\text{max}}/\sigma_0 = 7.0^{+2.5}_{-2.8}$  for U4-16795 and  $4.1^{+1.7}_{-1.5}$  for U4-16504.

#### 4. DUST AND GAS MASS ESTIMATES

##### 4.1. Dust mass

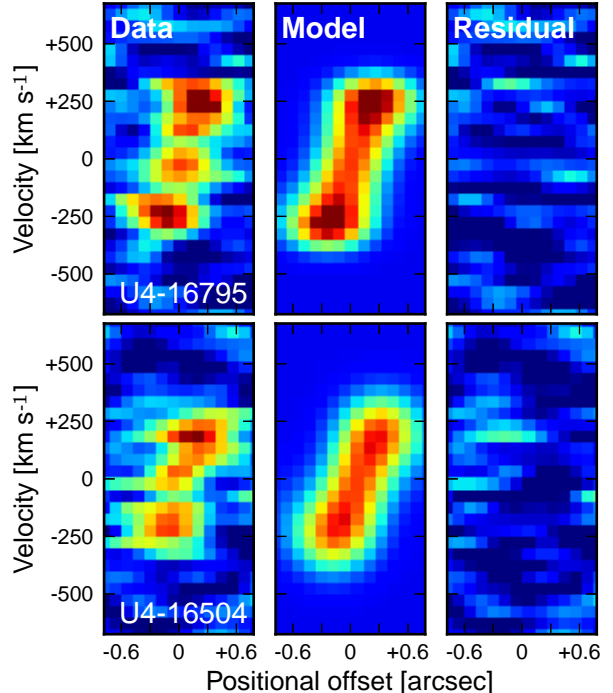


FIG. 3.— Observed position-velocity diagrams of the CO spectra (left). The middle and right panels show the best-fit dynamical model and the residuals between the data and the model, respectively.

Rest-frame  $850\ \mu\text{m}$  continuum emission is a good indicator of dust mass,  $M_{\text{dust}}$ . For galaxies at  $z \sim 2$ , rest-frame  $850\ \mu\text{m}$  fluxes are often extrapolated from  $\sim 1$  mm fluxes using a modified-blackbody radiation (MBB) model with dust temperature of  $T_d=25$  K and the dust emissivity,  $\kappa \propto \nu^\beta$ , with an index of  $\beta = 1.8$  (e.g., Scoville et al. 2016) as

$$S_\nu = \frac{M_{\text{dust}} \kappa_{\nu_{\text{rest}}} B_{\nu_{\text{rest}}}(T_d)(1+z)}{d_L^2}, \quad (1)$$

where  $d_L$  is the luminosity distance. We directly measure the rest-frame  $850\ \mu\text{m}$  fluxes from the 3 mm continuum and validate the extrapolation from the  $870\ \mu\text{m}$  continuum. Making  $870\ \mu\text{m}$  maps with the same synthesized beam as the 3 mm maps, we measure peak fluxes of  $S_{870\ \mu\text{m}} = 3.5 \pm 0.1$   $\text{mJy beam}^{-1}$  for U4-16795 and  $S_{870\ \mu\text{m}} = 2.2 \pm 0.1$   $\text{mJy beam}^{-1}$  for U4-16504. They correspond to 77% and 78% of the total flux within a  $1''.5$  aperture. Although the MBB models give the extrapolated fluxes of  $S_{3\text{mm}} = 90 \pm 3$   $\mu\text{Jy beam}^{-1}$  for U4-16795 and  $S_{3\text{mm}} = 55 \pm 3$   $\mu\text{Jy beam}^{-1}$  for U4-16504, we do not detect the 3 mm continuum emission above  $5\sigma$  significance ( $\sim 42$   $\mu\text{Jy beam}^{-1}$  and  $\sim 45$   $\mu\text{Jy beam}^{-1}$ , respectively).

Focusing on U4-16795, we evaluate the assumption of  $T_d$  and  $\beta$  with the MBB model. In addition to the flux measurements at PACS  $160\ \mu\text{m}$ , ALMA  $870\ \mu\text{m}$ , and the upper limit at ALMA 3 mm, we use the ALMA 1.1 mm flux ( $S_{1.1\text{mm}} = 1.75 \pm 0.07$   $\text{mJy beam}^{-1}$ ; Tadaki et al. 2015). Figure 4 shows several MBB models with different dust temperature and emissivity index. The  $5\sigma$  upper limit at 3 mm immediately rejects the models with  $T_d=25$  K, suggesting a higher  $T_d$  or a steeper  $\beta$ .

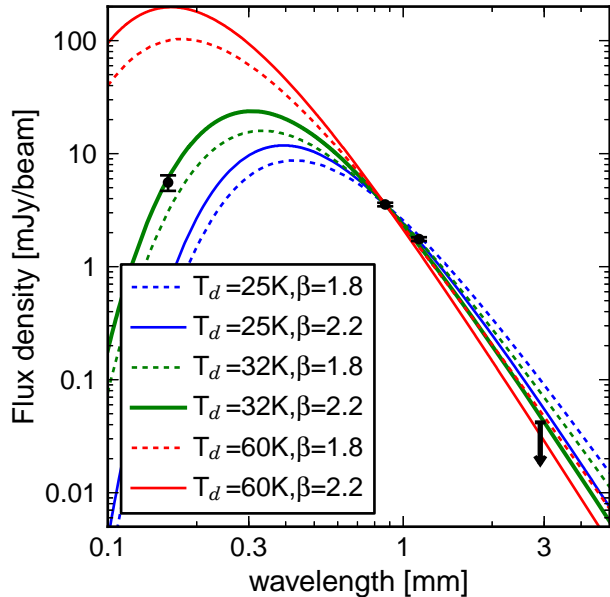


FIG. 4.— Dust continuum SED for U4-16795 with several types of modified blackbody radiation models. The black points are the fluxes measured at PACS 160  $\mu\text{m}$ , ALMA 870  $\mu\text{m}$ , and 1.1 mm. The upper limit is given by the  $5\sigma$  flux at ALMA 3 mm.

MBB models with an emissivity index in the usual range ( $\beta = 1.5 - 2.0$ ; Dunne & Eales e.g., 2001) require a much higher dust temperature of  $T_d > 60$  K to explain the faint 3 mm flux while they are inconsistent with the 160  $\mu\text{m}$  flux. Therefore, we reasonably assume  $T_d = 33$  K and  $\beta = 2.2$  to explain all data points. In the range of the dust emissivity of  $\kappa_{850} = 0.4 - 1.5 \text{ g}^{-1} \text{cm}^2$  at the rest-frame 850  $\mu\text{m}$  (Dunne et al. 2003), the  $5\sigma$  limits of the total dust mass are  $\log(M_{\text{dust},5\sigma}/M_\odot) = 8.30 - 8.88$  for U4-16795 and  $\log(M_{\text{dust},5\sigma}/M_\odot) = 8.33 - 8.90$  for U4-16504. If we use the 870  $\mu\text{m}$  flux assuming  $T_d = 25$  K and  $\beta = 1.8$ , the estimated dust mass would become larger by 0.5 dex.

#### 4.2. Gas mass

We estimate the CO-based gas masses using two conversion factors,  $\alpha_{\text{CO}} = 4.36 M_\odot (\text{K km s}^{-1} \text{pc}^{-2})^{-1}$  (Galactic value) and  $\alpha_{\text{CO}} = 0.8 M_\odot (\text{K km s}^{-1} \text{pc}^{-2})^{-1}$  (starburst value; Downes & Solomon 1998). We then compare the gas masses derived with these two different conversion factors to the dynamical and stellar masses. The CO  $J = 3 - 2$  emission line is assumed to be thermalized (Bolatto et al. 2015). These mass measurements are summarized in Table 1. If we adopt the Galactic conversion factor, the baryonic mass fraction, defined as  $f_{\text{bar}} = (M_* + M_{\text{gas}})/M_{\text{dyn}}$ , exceeds unity, which is in the unphysical regime. Monte Carlo simulations incorporating the uncertainties of gas, stellar and dynamical mass show that the probability of the baryonic mass fraction being in the physical regime is 2.3% for U4-16795 and 17.1% for U4-16504. In the case of the starburst conversion factor, the probability is increased to 24.7% and 55.3%, respectively. Thus, with regard to mass budget of massive galaxy cores in formation, the starburst conversion factor is preferred over the Galactic.

We also independently constrain the gas mass from the 3 mm-based dust mass, assuming a gas-to-dust ratio of

120 which is the average value in central regions of local LIRG/ULIRGs (Wilson et al. 2008). The  $5\sigma$  upper limit is  $\log(M_{\text{gas},5\sigma}/M_\odot) < 11$  (Table 1), supporting the starburst conversion factor. Therefore, we adopt the starburst conversion factor to derive the CO-based gas mass. Then, the gas-to-dynamical mass fraction is  $15^{+4}_{-5}\%$  for U4-16795 and  $12^{+4}_{-5}\%$  for U4-16504 and the gas depletion timescale is  $M_{\text{gas}}/SFR = 46 \pm 11$  Myr and  $79 \pm 46$  Myr, respectively, which is comparable to those of optically compact star-forming galaxies (Barro et al. 2016).

## 5. DISCUSSION AND SUMMARY

Using ALMA observations of CO  $J = 3 - 2$  emission, we find that the compact molecular gas in the star-forming cores of two massive galaxies is rotating. This has implications for both the formation and subsequent evolution of the cores of massive galaxies. The formation mechanism appears to be dissipative and the observed rotation indicates that at least some angular momentum is preserved in the star-forming molecular gas. Simulations show this could happen due to a gas-rich merger or disk instabilities (e.g., Zolotov et al. 2015; Wellons et al. 2015). Given the short gas depletion time and the fact that their stellar masses are nearly the Schechter mass, these galaxies likely represent the immediate progenitors of the massive quiescent galaxies with dense cores at  $z \sim 2$ . Kinematic studies of massive quiescent galaxies suggest they are rotating (Newman et al. 2015), although with lower  $v/\sigma$  than found here for their progenitors. Additionally, the descendants of these galaxies in the local universe are elliptical “slow rotators” with  $v/\sigma$  nearly an order of magnitude lower (Cappellari 2016), suggesting that the galaxies we observe need to lose significant net angular momentum in the intervening time. Our results support a picture in which net angular momentum is initially reduced during the quenching process and further during a growth phase by dry mergers.

We find that the molecular gas of the two massive galaxies at  $z = 2.5$  is compact with  $R_e \sim 2$  kpc, which is a factor of two smaller than the optical size of star-forming galaxies at similar stellar mass. Such a concentration of star-forming gas is consistent with a scenario in which a wet compaction events (radial transport of gas) could build the cores of massive galaxies (Zolotov et al. 2015). The two galaxies host even more compact starbursts with a high SFR surface density as traced by the dust continuum emission, rapidly building up dense cores and transforming the galaxy morphology from disk-dominated to bulge-dominated (Tadaki et al. 2017).

Our independent measurements of dynamical, stellar, gas and dust mass suggest that the starburst CO-to- $\text{H}_2$  conversion factor is appropriate for the spatially resolved cores. These dense cores are likely to be formed in extreme environments like central regions of local ULIRGs. The same conclusion is obtained by recent [C I] observations of a star-forming galaxy in the similar mass and redshift range (Popping et al. 2017) and CO observations of starburst galaxies above the main-sequence (Sargent et al. 2014). On the other hand, it is not clear yet that the starburst conversion factor is appropriate for entire galaxies. Tacconi et al. (2017) investigated the variations in molecular gas properties for 650 galaxies over  $0 < z < 3$  by compiling CO and dust continuum

data and does not find the presence of such a large change in the conversion factor. A statistical study of the kinematics of the molecular gas is an essential next step for getting a consensus on this issue. However, high-spatial resolution CO observations suffer from missing flux and are more time-consuming compared to dust continuum observations. A combination of medium-resolution CO and high-resolution dust continuum observations is reasonable in terms of observing time and a powerful tool for characterizing the dynamical state of molecular gas in distant galaxies.

This paper makes use of the following ALMA data:

ADS/JAO.ALMA#2013.1.00742.S. ALMA is a partnership of ESO (representing its member states), NSF (USA) and NINS (Japan), together with NRC (Canada), NSC and ASIAA (Taiwan), and KASI (Republic of Korea), in cooperation with the Republic of Chile. The Joint ALMA Observatory is operated by ESO, AUI/NRAO and NAOJ. K.T. was supported by the ALMA Japan Research Grant of NAOJ Chile Observatory, NAOJ-ALMA-57. This paper is produced as a part of our collaborations through the joint project supported by JSPS and DAAD under the Japan - German Research Cooperative Program.

#### REFERENCES

- Barro, G., Trump, J. R., Koo, D. C., et al. 2014, *ApJ*, 795, 145, 145
- Barro, G., Kriek, M., Pérez-González, P. G., et al. 2016, *ApJ*, 827, L32, L32
- Belli, S., Newman, A. B., & Ellis, R. S. 2015, *ApJ*, 799, 206, 206
- Bolatto, A. D., Wolfire, M., & Leroy, A. K. 2013, *ARA&A*, 51, 207, 207
- Bolatto, A. D., Warren, S. R., Leroy, A. K., et al. 2015, *ApJ*, 809, 175, 175
- Bruzual, G., & Charlot, S. 2003, *MNRAS*, 344, 1000, 1000
- Burkert, A., Genzel, R., Bouché, N., et al. 2010, *ApJ*, 725, 2324, 2324
- Calzetti, D., Armus, L., Bohlin, R. C., et al. 2000, *ApJ*, 533, 682, 682
- Cappellari, M. 2016, *ARA&A*, 54, 597, 597
- Chabrier, G. 2003, *PASP*, 115, 763, 763
- Davies, R., Förster Schreiber, N. M., Cresci, G., et al. 2011, *ApJ*, 741, 69, 69
- Downes, D., & Solomon, P. M. 1998, *ApJ*, 507, 615, 615
- Dunne, L., Eales, S., Ivison, R., Morgan, H., & Edmunds, M. 2003, *Nature*, 424, 285, 285
- Dunne, L., & Eales, S. A. 2001, *MNRAS*, 327, 697, 697
- Fang, J. J., Faber, S. M., Koo, D. C., & Dekel, A. 2013, *ApJ*, 776, 63, 63
- Fontana, A., Dunlop, J. S., Paris, D., et al. 2014, *A&A*, 570, A11, A11
- Hodge, J. A., Swinbank, A. M., Simpson, J. M., et al. 2016, *ApJ*, 833, 103, 103
- Ivison, R. J., Swinbank, A. M., Smail, I., et al. 2013, *ApJ*, 772, 137, 137
- Kriek, M., van Dokkum, P. G., Labbé, I., et al. 2009, *ApJ*, 700, 221, 221
- Law, D. R., Steidel, C. C., Erb, D. K., et al. 2009, *ApJ*, 697, 2057, 2057
- Lutz, D., Poglitsch, A., Altieri, B., et al. 2011, *A&A*, 532, A90, A90
- Martí-Vidal, I., Vlemmings, W. H. T., Muller, S., & Casey, S. 2014, *A&A*, 563, A136, A136
- McMullin, J. P., Waters, B., Schiebel, D., Young, W., & Golap, K. 2007, in *Astronomical Society of the Pacific Conference Series*, Vol. 376, *Astronomical Data Analysis Software and Systems XVI*, ed. R. A. Shaw, F. Hill, & D. J. Bell, 127
- Narayanan, D., Krumholz, M. R., Ostriker, E. C., & Hernquist, L. 2012, *MNRAS*, 421, 3127, 3127
- Nelson, E., van Dokkum, P., Franx, M., et al. 2014, *Nature*, 513, 394, 394
- Nelson, E. J., van Dokkum, P. G., Momcheva, I. G., et al. 2016, *ApJ*, 817, L9, L9
- Newman, A. B., Belli, S., & Ellis, R. S. 2015, *ApJ*, 813, L7, L7
- Onodera, M., Carollo, C. M., Renzini, A., et al. 2015, *ApJ*, 808, 161, 161
- Popping, G., Decarli, R., Man, A. W. S., et al. 2017, *ArXiv e-prints*, arXiv:1703.05764
- Sargent, M. T., Daddi, E., Béthermin, M., et al. 2014, *ApJ*, 793, 19, 19
- Scoville, N., Sheth, K., Aussel, H., et al. 2016, *ApJ*, 820, 83, 83
- Skelton, R. E., Whitaker, K. E., Momcheva, I. G., et al. 2014, *ApJS*, 214, 24, 24
- Speagle, J. S., Steinhardt, C. L., Capak, P. L., & Silverman, J. D. 2014, *ApJS*, 214, 15, 15
- Tacconi, L. J., Genzel, R., Smail, I., et al. 2008, *ApJ*, 680, 246, 246
- Tacconi, L. J., Genzel, R., Saintonge, A., et al. 2017, *ArXiv e-prints*, arXiv:1702.01140
- Tadaki, K.-i., Kodama, T., Tanaka, I., et al. 2013, *ApJ*, 778, 114, 114
- Tadaki, K.-i., Kohno, K., Kodama, T., et al. 2015, *ApJ*, 811, L3, L3
- Tadaki, K.-i., Genzel, R., Kodama, T., et al. 2017, *ApJ*, 834, 135, 135
- van der Wel, A., Franx, M., van Dokkum, P. G., et al. 2014a, *ApJ*, 788, 28, 28
- van der Wel, A., Chang, Y.-Y., Bell, E. F., et al. 2014b, *ApJ*, 792, L6, L6
- van Dokkum, P. G., Bezanson, R., van der Wel, A., et al. 2014, *ApJ*, 791, 45, 45
- Wellons, S., Torrey, P., Ma, C.-P., et al. 2015, *MNRAS*, 449, 361, 361
- Wilson, C. D., Petitpas, G. R., Iono, D., et al. 2008, *ApJS*, 178, 189, 189
- Wisnioski, E., Förster Schreiber, N. M., Wuyts, S., et al. 2015, *ApJ*, 799, 209, 209
- Wuyts, S., Förster Schreiber, N. M., van der Wel, A., et al. 2011a, *ApJ*, 742, 96, 96
- Wuyts, S., Förster Schreiber, N. M., Lutz, D., et al. 2011b, *ApJ*, 738, 106, 106
- Wuyts, S., Förster Schreiber, N. M., Genzel, R., et al. 2012, *ApJ*, 753, 114, 114
- Wuyts, S., Förster Schreiber, N. M., Wisnioski, E., et al. 2016, *ApJ*, 831, 149, 149
- Zolotov, A., Dekel, A., Mandelker, N., et al. 2015, *MNRAS*, 450, 2327, 2327